Supplement of

Surfactants Regulate the Mixing State of Organic-Inorganic Mixed Aerosols Undergoing Liquid-Liquid Phase Separation

Younuo Fan,[a] Qiong Li,[a,b,*] Min Zhou,[a,c] Jiuyi Sun,[d] Shuaishuai Ma,[a,*] Tianyou Xu[a]

[a] *College of Chemical and Material Engineering, Quzhou University, Quzhou 324000, China*

[b] *Shanghai Key Laboratory of Atmospheric Particle Pollution and Prevention, Department of Environmental Science & Engineering, Fudan University, Shanghai 200433, China*

[c] *College of Chemical Engineering, Zhejiang University of Technology, Hangzhou 310000, China*

[d] *The Institute of Chemical Physics, School of Chemistry and Chemical Engineering, Beijing Institute of Technology, Beijing 100081, China*

Numbers of pages: 32

Numbers of Figures: 18

[*] Email: lq270224181@126.com; mass@qzc.edu.cn Phone: 86-570-8026552 Fax: 86-570-8026552

Table of Contents

Figure S6. SDS concentration evolutions predicted by the EAIM model (a) and surface tension measurements from simulated SDS/AS mixed solutions (b) as a function of ambient RH for particles with org:sulf:SDS ratios of 1:1:0.001, 1:4:0.0075, and 4:1:0.0045. AS and SDS concentrations in the simulated SDS/AS solutions are derived from EAIM predictions. Each surface tension measurement represents the average of three replicates.

Figure S7. Optical images and corresponding illustrations of mixed 1,2,6-hexanetriol/AS/SDS particles with org:sulf:SDS ratios of 1:1:0.005 and 1:1:0.01 after LLPS and efflorescence. The RH percentage is indicated in each frame.

Figure S8. Optical images and corresponding illustrations of mixed 1,2,6-hexanetriol/AS/SDS particles with org:sulf:SDS ratios of 1:1:0.1 (a) and 1:1:1 (b) during LLPS, efflorescence, and deliquescence. The RH percentage is indicated in each frame, with specific values highlighted in red to signify the occurrence of phase transitions.

Figure S9. Optical images and corresponding illustrations of mixed 1,2,6-hexanetriol/AS/SDS particles with org:sulf:SDS ratios of 1:1:0.001 (a), 1:1:0.005 (b), 1:1:0.2 (c), and 1:1:0.5 (d) after LLPS and efflorescence. The corresponding RH values during dehumidification are indicated in each frame. Note that the illustrations depict only the biphasic particles with identifiable mixing states.

Figure S10. Optical images and corresponding illustrations of mixed 1,2,6-hexanetriol/AS/SDS particles with an org:sulf:SDS ratio of 1:1:0.01, obtained from mixture solutions at pH 1.5, during LLPS, efflorescence, and deliquescence. The RH percentage is indicated in each frame, with specific values highlighted in red to signify the occurrence of phase transitions.

Figure S11. Optical images and corresponding illustrations of mixed organic/AS/SDS particles with an org:sulf:SDS ratio of 1:1:0.01 after LLPS.

Figure S12. Optical images and corresponding illustrations of mixed 1,2,6-hexanetriol/AS/CTAC particles with org:sulf:CTAC ratios of 1:1:0.00001 (a) and 1:1:0.005 (b) during LLPS, efflorescence, and deliquescence. The RH percentage is indicated in each frame, with specific values highlighted in red to signify the

occurrence of phase transitions. (c) Equilibrium particle morphologies after LLPS for 1,2,6-hexanetriol/AS/CTAC particles at different initial CTAC concentrations.

Figure S13. Surface tension measurements at varying concentrations of CTAC and SDS for simulated CTAC/AS and SDS/AS mixed solutions, with a fixed AS concentration of 2.71 mol L^{-1}. Hollow symbols indicate estimated approximate surface tension values.

Figure S14. Optical images and corresponding illustrations of mixed 1,2,6-hexanetriol/AS/Triton X-100 particles with varying org:sulf:Triton X-100 ratios after LLPS.

Figure S15. Optical images and corresponding illustrations of mixed 1,2,6-hexanetriol/AS/PFOA particles with the molar ratio of 1:1:0.1 during LLPS, efflorescence, and deliquescence. The RH percentage is indicated in each frame, with specific values highlighted in red to signify the occurrence of phase transitions.

Figure S16. Calculated spreading coefficients, S_1 and S_2, as a function of surfactant concentration for model systems of octane/AS (a) and octanol/AS (b) with the addition of SDS, CTAC, or Triton X-100.

Figure S17. SRH (a) and ERH (b) values for OIR = 1:4, 1:1, and 4:1 particles with varying initial concentrations of SDS, CTAC, and Triton X-100. The dotted lines indicate the original SRH and ERH values for 1,2,6-hexanetriol/AS mixed particles without surfactants.

Figure S18. Optical images of pure SDS system during an RH cycle. The RH percentage is indicated in each frame.

S1. Influence of SDS on the Mixing State of OIR = 1:4 and 4:1 Particles

For the particle with OIR = 1:4 without SDS, LLPS occurs via the growth of a second phase from the particle surface at RH values between 74.3% and 70.9% (Figure S3a). Following efflorescence, the organic phase becomes trapped within the cavity of the AS crystal. These scenarios are consistent with our previous observations (Ma et al., 2021a). Upon adding SDS, the LLPS mechanism changes to spinodal decomposition, as depicted in Figure S3b and S3c. During this process, schlieren patterns appear over the aqueous droplet, followed by the growth and coalescence of separated AS inclusions (Ma et al., 2021a; Ciobanu et al., 2009). Notably, as the SDS fraction increases, such as in the org:sulf:SDS = 1:4:0.0075 mixture, a core-shell morphology is no longer observed; instead, a partial engulfing structure forms (Figure S3c). Further increases in SDS concentration, seen in the 1:4:0.008 and 1:4:0.01 mixtures (Figure S4a and S4b), still result in the persistence of partial organic-phase engulfing.

Figure S5 illustrates the phase transition behaviors of mixed 1,2,6-hexanetriol/AS/SDS particles with org:sulf:SDS ratios of 4:1:0.004, 4:1:0.0045, and 4:1:0.005. For the 4:1:0.004 mixture, LLPS occurs at 77.9% RH through a nucleation and growth mechanism (Ma et al., 2021a; Ciobanu et al., 2009), resulting in a core-shell particle morphology. In contrast, for the 4:1:0.0045 and 4:1:0.005 mixtures, LLPS occurs via spinodal decomposition, leading to the formation of numerous dispersed AS inclusions. Coupled with the particle morphologies observed

after efflorescence, we can infer that these AS inclusions tend to reside on the particle surface, indicative of a partial engulfing structure.

It is evident that the SDS concentration threshold regulating the dominance of core-shell versus partial engulfing morphologies differs between the OIR = 1:4 and 4:1 systems compared to the OIR = 1:1 particles. To further explore this, we compare the changes in SDS concentration and surface tension with decreasing RH for the org:sulf:SDS = 1:1:0.001, 1:4:0.0075, and 4:1:0.0045 systems, as shown in Figure S6. At the SRH, the three systems exhibit distinct SDS concentrations of 2.71, 7.27, and 5.10 mM, with corresponding surface tensions of 68.49, 53.15, and 25.10 mN m^{-1}, respectively. These discrepancies imply a complex correlation between particle OIR and the surfactant concentration thresholds.

The change in total surface free energy (G_s) during spreading depends not only on the spreading coefficients (S_i) but also on the changes in surface and interface areas of the organic and inorganic phases (dA) (Torza and Mason, 1970; Shaw, 1992):

$$dG_s = -S_i dA \quad \text{(S1)}$$

Thus, while the three systems have varying concentrations of organic and inorganic phases, resulting in distinct surface and interfacial tensions during LLPS, the differences in SDS concentration thresholds can be partially attributed to different volume ratios. This is another key factor affecting total surface free energy, in addition to interfacial tensions. Similar to previous studies, our findings emphasize the importance of considering both interfacial tensions and the volumes of separated

phases, related to particle OIR, for accurately predicting final particle morphology (Kwamena et al., 2010).

S2. Surface Tension Predictions for Aqueous Systems with Decreasing RH

Wexler and Dutcher (2013) developed an equation based on statistical mechanics to describe the relationship between the surface tension (σ) of a solution and solute activity (a_A):

$$\sigma = \sigma_W + \frac{kT}{rS_W} \ln\left(\frac{1-Ka_A}{1-Ka_A(1-C)}\right) \quad \text{(S2)}$$

where σ_W is the surface tension of pure water (N m^{-1}), k is Boltzmann's constant (J K^{-1}), T is the ambient temperature (K), and S_W is the area occupied by a water molecule, typically assumed to be 0.1 nm^2. The remaining three unknown parameters, r, K, and C, are specific to each solute, with r representing the average number of water molecules displaced from the surface by each solute molecule, while K and C relate to sorption energies.

For aqueous AS solution, Boyer et al. (2015) estimated values of r = -4.04 and K = 0.99, based on electrolyte fits using Equation (S2). Coupled with the surface tension of pure solute (σ_S = 184.99 mN m^{-1} for molten AS) (Dutcher et al., 2010), the parameter C is calculated as 670.39 using the formula $C = 1 - [1 - (1 - K)\exp(rS_W(\sigma_W - \sigma_S)/kT)]/K$ (Wexler and Dutcher, 2013). Therefore, the surface tension of sulfate-containing aqueous droplets can be predicted as a function of solute activity, which varies with decreasing RH, based on the evolution of AS concentration.

Dutcher et al. (2011) extended the Brunauer-Emmett-Teller (BET) and Guggenheim-Anderson-de Boer (GAB) adsorption models to account for additional

adsorbed monolayers when determining solute and solvent activities in aqueous solutions over a wide concentration range. Assuming each solute entity is surrounded by three hydrated layers of water molecules, the solute molality (m_A) can be expressed as a function of water activity (a_W) according to the three-layer model (Dutcher et al., 2011):

$$m_A = \left(\frac{1-a_W K_A}{M_W r_A C_{A,1} a_W K_A}\right)\left(\frac{1-K_A a_W(1-C_{A,1})-K_A^2 a_W^2 C_{A,1}(1-C_{A,2})}{(1-a_W K_A)^2+(2-a_W K_A)a_W K_A C_{A,2}}\right) \quad \text{(S3)}$$

The solute activity (a_A) can also be expressed as a function of water activity (a_W) (Dutcher et al., 2011):

$$a_A = \left(\frac{1-K_A a_W}{1-K_A a_W(1-C_{A,1})-K_A^2 a_W^2 C_{A,1}(1-C_{A,2})}\right)^{r_A} \quad \text{(S4)}$$

Here, M_W is the molecular weight of water (the adsorbate) (kg mol^{-1}), r_A represents the number of adsorption sites on solute A, while K_A, $C_{A,1}$, and $C_{A,2}$ are energy parameters related to the exponent of the difference between the energy of adsorption to a layer and the bulk energy of liquefaction. In Dutcher's later work, the values for the aqueous AS solution were determined to be r_A = 1.872, K_A = 0.9876, $C_{A,1}$ = 0.0812, and $C_{A,2}$ = 34.77 (Dutcher et al., 2013). Using the EAIM model, the molality of aqueous AS across the entire RH range for the OIR = 1:1 system can be simulated, allowing a_W and a_A at specific RH levels to be calculated using Equations (S3) and (S4). Combined with the relationship between surface tension and solute activity in Equation (S2), the surface tension of the mixed droplets (org:sulf:SDS = 1:1:0.001) can be predicted, considering only AS concentration changes as RH decreases.

For the contribution of SDS to droplet surface tension, the empirical Szyskowski equation can be applied (Szyskowski, 1908):

$$\sigma = \sigma_{\mathrm{W}} - a\mathrm{In}\left(1 + \frac{c_{\mathrm{SDS}}}{b}\right) \quad \text{(S5)}$$

where c_{SDS} is the concentration of SDS (mol L^{-1}), and parameters a and b are determined by fitting surface tension data of pure SDS solutions, measured using the hanging droplet method (Figure 3c). The evolution of SDS concentration with decreasing RH is evaluated based on the fixed molar ratio of AS to SDS.

When considering both AS and SDS contributions, the surface tension parametrization for the ternary SDS/AS aqueous solution is obtained with the modified Szyskowski equation (Prisle et al., 2010):

$$\sigma = \sigma_{\mathrm{W}} + (\frac{d\sigma_{\mathrm{AS}}}{dc_{\mathrm{AS}}})c_{\mathrm{AS}} - a\mathrm{In}\left(1 + \frac{c_{\mathrm{SDS}}(c_{\mathrm{AS}}+b_2)}{b_1}\right) \quad \text{(S6)}$$

As the solutions are dilute, the gradient of surface tension for aqueous AS (σ_{AS}) with respect to its molar concentration (c_{AS}), denoted by $(\frac{d\sigma_{\mathrm{AS}}}{dc_{\mathrm{AS}}})$, was measured to be 2.362 mN m^{-1}/mol L^{-1} (Svenningsson et al., 2006). Surface tension depression in SDS/AS aqueous solutions was determined for fixed AS concentrations of 0, 0.1, or 1 mol L^{-1}, using the hanging droplet method (Figure 4c). The least squares method was applied to determine the optimal values of a, b_1, and b_2. Consequently, the surface tension can be estimated for specific AS and SDS concentrations at given RH levels, as predicted by the EAIM model.

S3. Changes in SRH and ERH with Varying Initial Surfactant Concentrations

Figure S17 illustrates the changes in SRH and ERH values for OIR = 1:4, 1:1, and 4:1 particles in the presence of surfactants (SDS, CTAC, and Triton X-100) at different initial concentrations, with 1,2,6-hexanetriol and AS set at 0.1 or 0.4 mol L^{-1}. The original SRH and ERH values for mixed particles without surfactants are assumed to be 76% and 45%, respectively. As shown in Figure S17a, at relatively low surfactant concentrations, surfactant molecules tended to form a thin organic layer on the particle surface, inhibiting water transport across the aqueous-air interface and reducing SRH values (Faust and Abbatt, 2019; Miñambres et al., 2014). For instance, the SRH of OIR = 1:1 particles decreases by approximately 9.0% with the addition of 0.001 mM CTAC. As surfactant concentration increases, the enhanced salting-out effect raises the SRH, reaching up to 90.6% RH for OIR = 1:1 particles with 100 mM Triton X-100.

In ERH measurements, low concentrations of ionic surfactants (SDS and CTAC) reduce the ERH of mixed particles (Figure S17b). For example, 0.001 mM CTAC lowers the ERH to 38.3% due to the inhibiting effect of the surface surfactant monolayer (Harmon et al., 2010). Conversely, high concentrations of ionic surfactants promote efflorescence of aqueous droplets at higher RH compared to the surfactant-free system. Considering the very high ERH of the pure SDS system (Figure S18), we infer that the SDS efflorescence induced the heterogenous nucleation of AS (Ma et al., 2021b). Additionally, Triton X-100 inhibits AS

efflorescence across the entire concentration range due to its lack of heterogenous efficacy.

Supplementary Figures

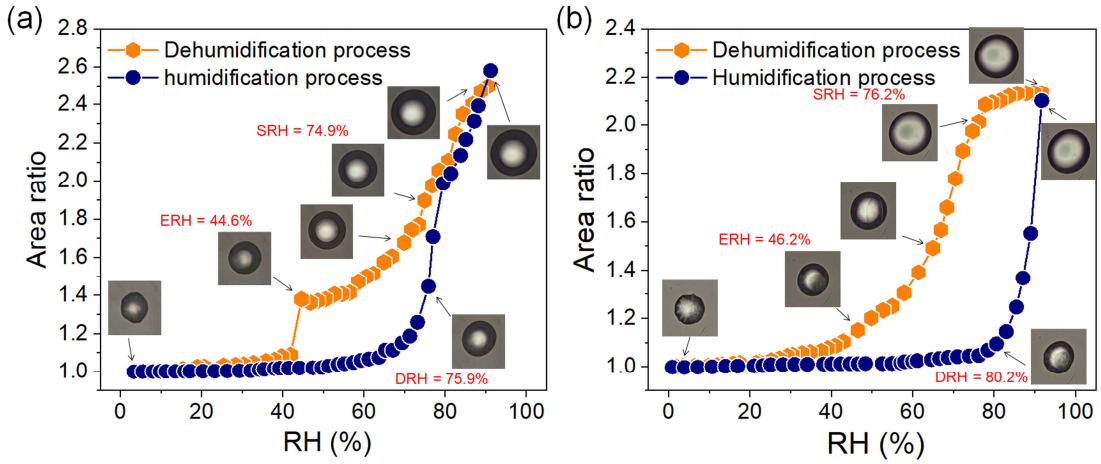

Figure S1. Hygroscopic growth curves for the OIR = 1:1 system without SDS (a) and the org:sulf:SDS = 1:1:0.001 system (b). The panels display optical images corresponding to area ratios at specific RH values. The SRH, ERH and DRH values are indicated in red.

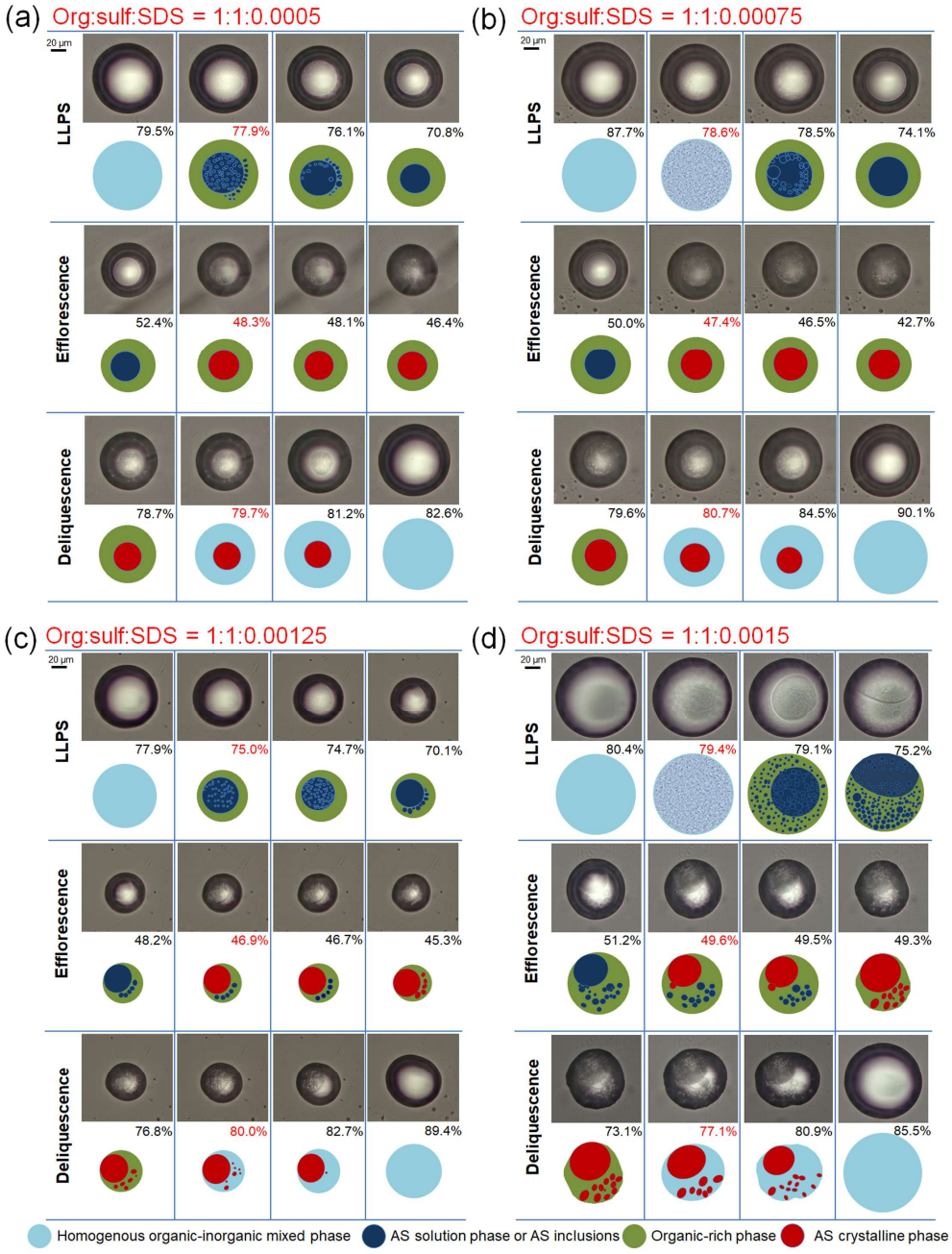

Figure S2. Optical images and corresponding illustrations of mixed 1,2,6-hexanetriol/AS/SDS particles with org:sulf:SDS ratios of 1:1:0.0005 (a), 1:1:0.00075 (b), 1:1:0.00125 (c), and 1:1:0.0015 (d) during LLPS, efflorescence, and deliquescence. The RH percentage is indicated in each frame, with specific values highlighted in red to signify the occurrence of phase transitions.

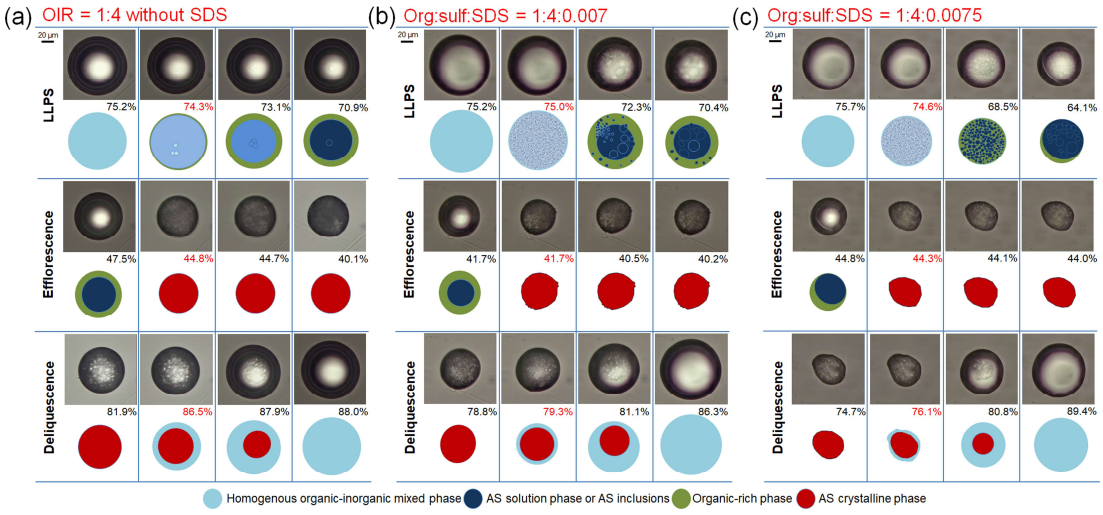

Figure S3. Optical images and corresponding illustrations of mixed 1,2,6-hexanetriol/AS particles with an OIR of 1:4 without SDS (a), and with org:sulf:SDS ratios of 1:4:0.007 (b) and 1:4:0.0075 (c), during LLPS, efflorescence, and deliquescence. The RH percentage is indicated in each frame, with specific values highlighted in red to signify the occurrence of phase transitions.

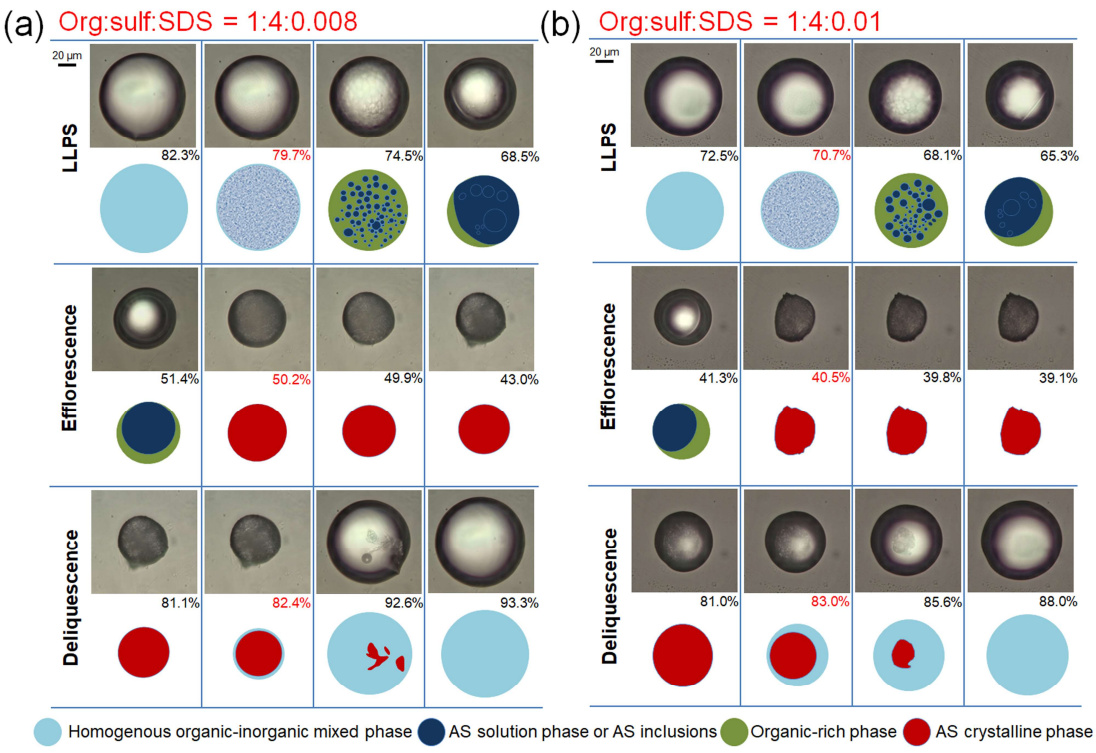

Figure S4. Optical images and corresponding illustrations of mixed 1,2,6-hexanetriol/AS/SDS particles with org:sulf:SDS ratios of 1:4:0.008 (a) and 1:4:0.01 (b) during LLPS, efflorescence, and deliquescence. The RH percentage is indicated in each frame, with specific values highlighted in red to signify the occurrence of phase transitions.

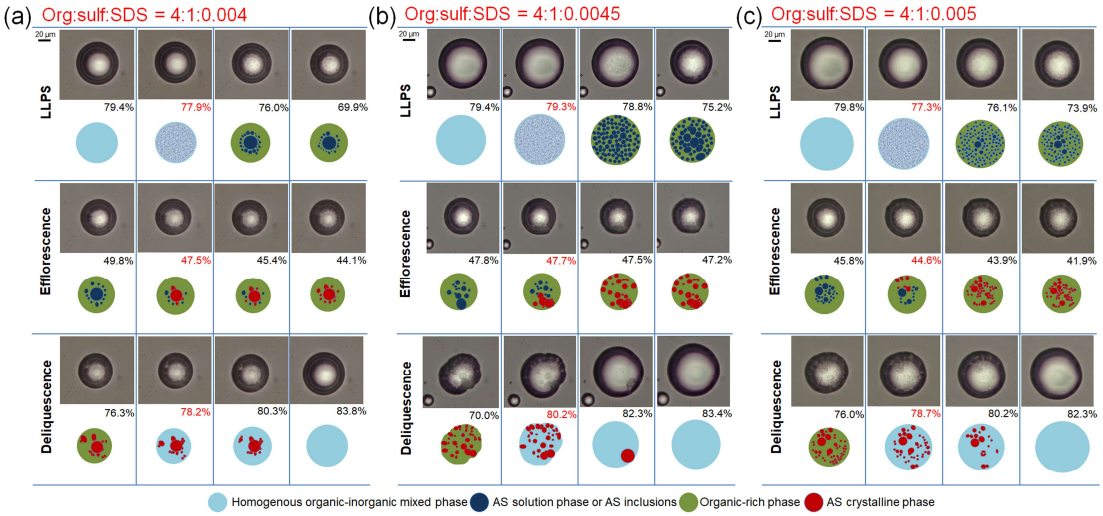

247

248 **Figure S5.** Optical images and corresponding illustrations of mixed 1,2,6-hexanetriol/AS/SDS
249 particles with org:sulf:SDS ratios of 4:1:0.004 (a), 4:1:0.0045 (b), and 4:1:0.005 (c) during LLPS,
250 efflorescence, and deliquescence. The RH percentage is indicated in each frame, with specific
251 values highlighted in red to signify the occurrence of phase transitions.

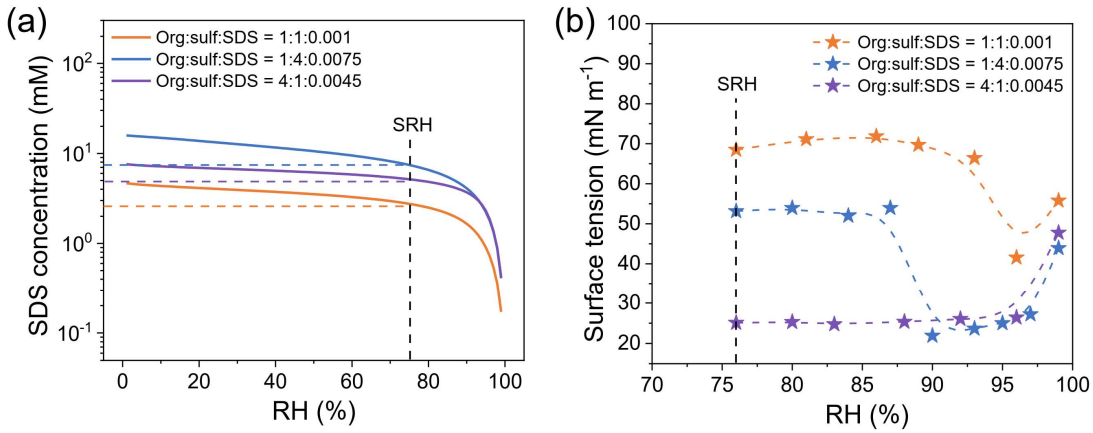

252

253 **Figure S6.** SDS concentration evolutions predicted by the EAIM model (a) and surface tension
254 measurements from simulated SDS/AS mixed solutions (b) as a function of ambient RH for
255 particles with org:sulf:SDS ratios of 1:1:0.001, 1:4:0.0075, and 4:1:0.0045. AS and SDS
256 concentrations in the simulated SDS/AS solutions are derived from EAIM predictions. Each
257 surface tension measurement represents the average of three replicates.

258

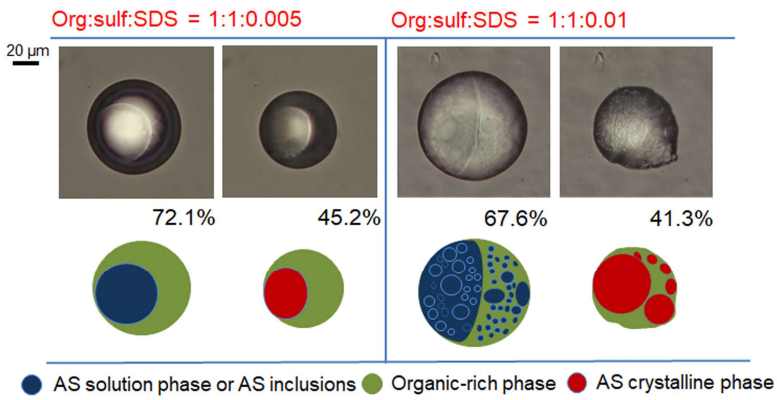

Figure S7. Optical images and corresponding illustrations of mixed 1,2,6-hexanetriol/AS/SDS particles with org:sulf:SDS ratios of 1:1:0.005 and 1:1:0.01 after LLPS and efflorescence. The RH percentage is indicated in each frame.

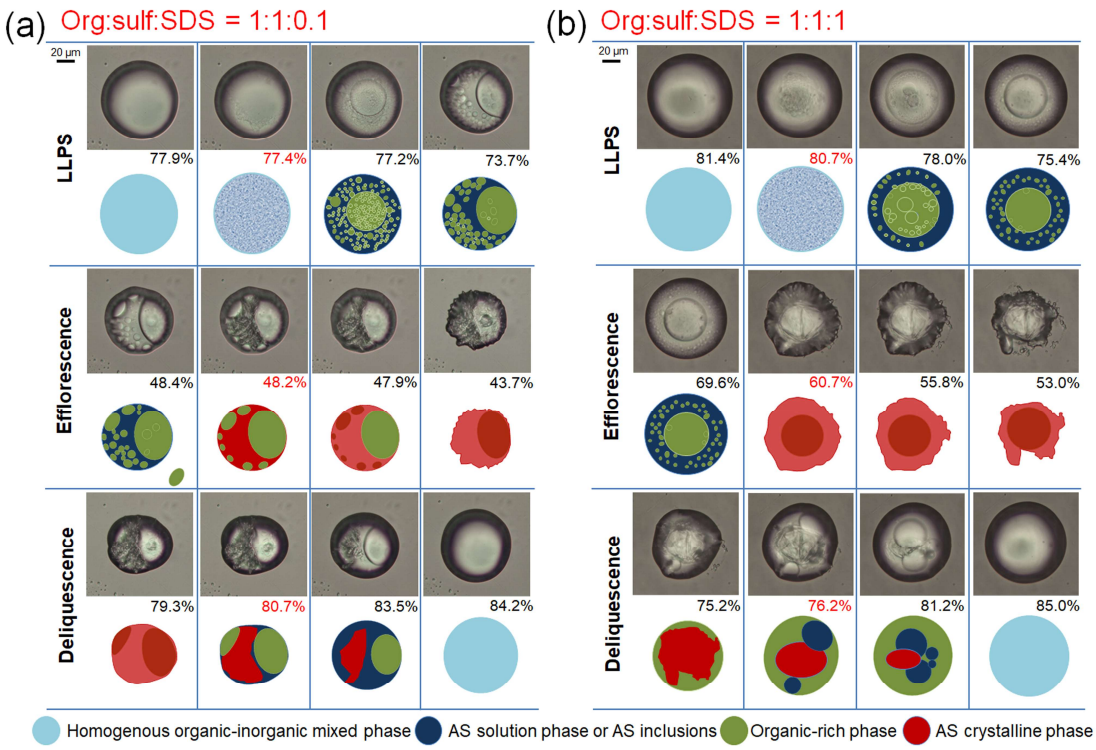

263

264 **Figure S8.** Optical images and corresponding illustrations of mixed 1,2,6-hexanetriol/AS/SDS
265 particles with org:sulf:SDS ratios of 1:1:0.1 (a) and 1:1:1 (b) during LLPS, efflorescence, and
266 deliquescence. The RH percentage is indicated in each frame, with specific values highlighted in
267 red to signify the occurrence of phase transitions.

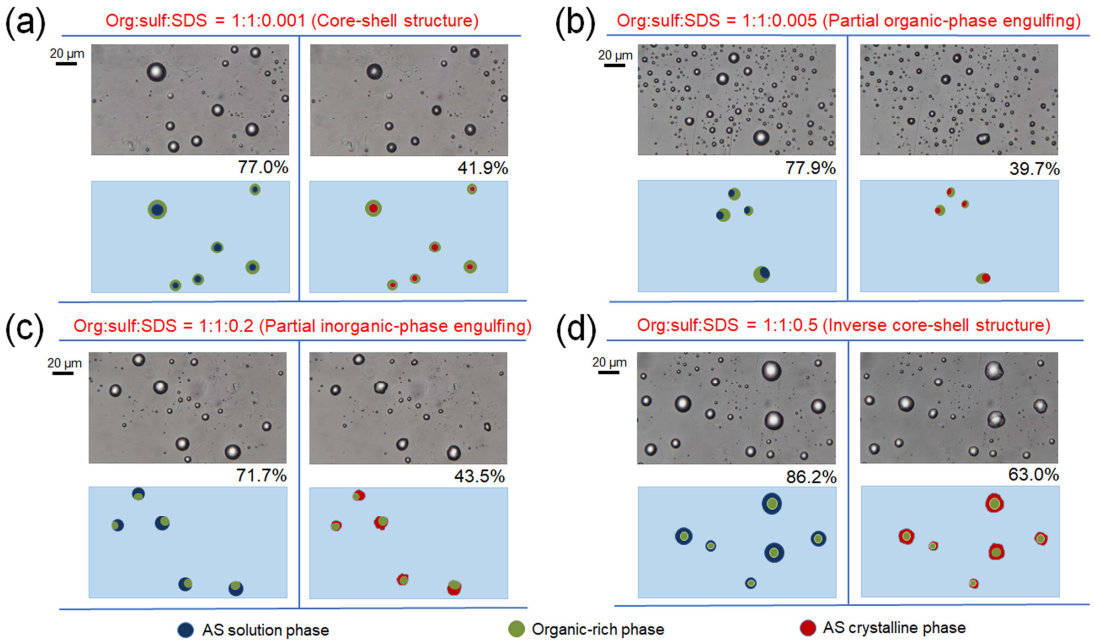

Figure S9. Optical images and corresponding illustrations of mixed 1,2,6-hexanetriol/AS/SDS particles with org:sulf:SDS ratios of 1:1:0.001 (a), 1:1:0.005 (b), 1:1:0.2 (c), and 1:1:0.5 (d) after LLPS and efflorescence. The corresponding RH values during dehumidification are indicated in each frame. Note that the illustrations depict only the biphasic particles with identifiable mixing states.

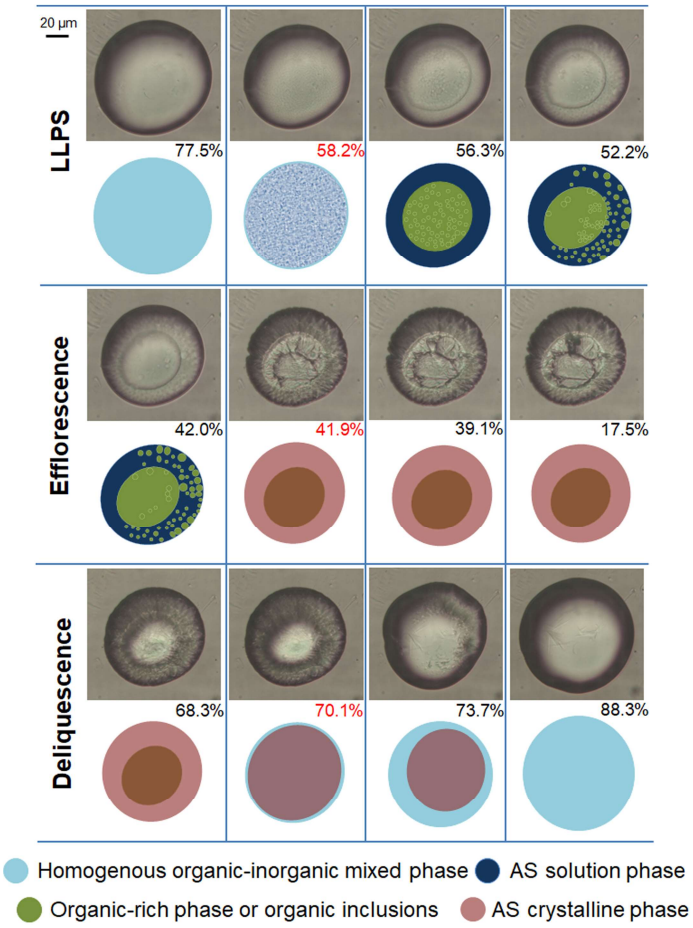

Figure S10. Optical images and corresponding illustrations of mixed 1,2,6-hexanetriol/AS/SDS particles with an org:sulf:SDS ratio of 1:1:0.01, obtained from mixture solutions at pH 1.5, during LLPS, efflorescence, and deliquescence. The RH percentage is indicated in each frame, with specific values highlighted in red to signify the occurrence of phase transitions.

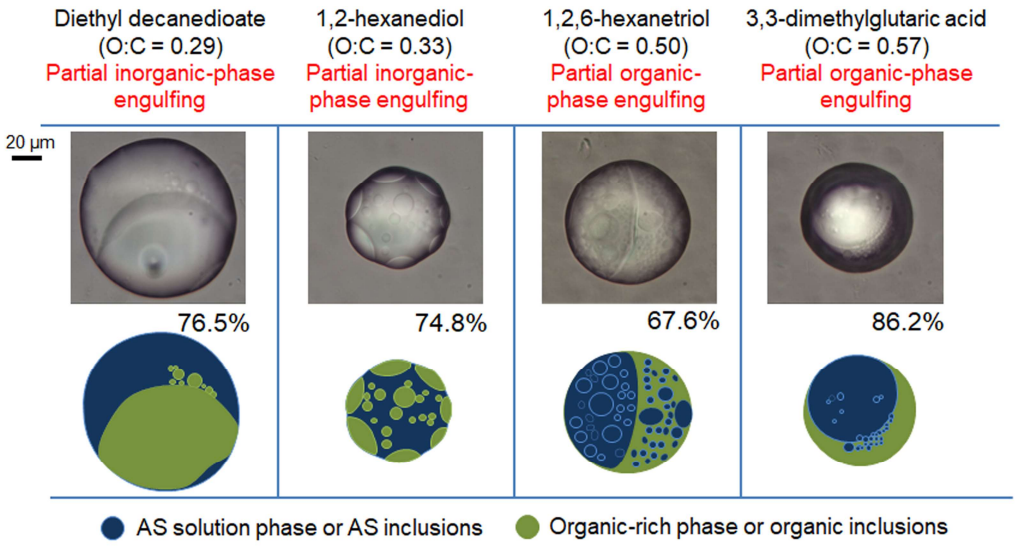

279

280 **Figure S11.** Optical images and corresponding illustrations of mixed organic/AS/SDS particles

281 with an org:sulf:SDS ratio of 1:1:0.01 after LLPS.

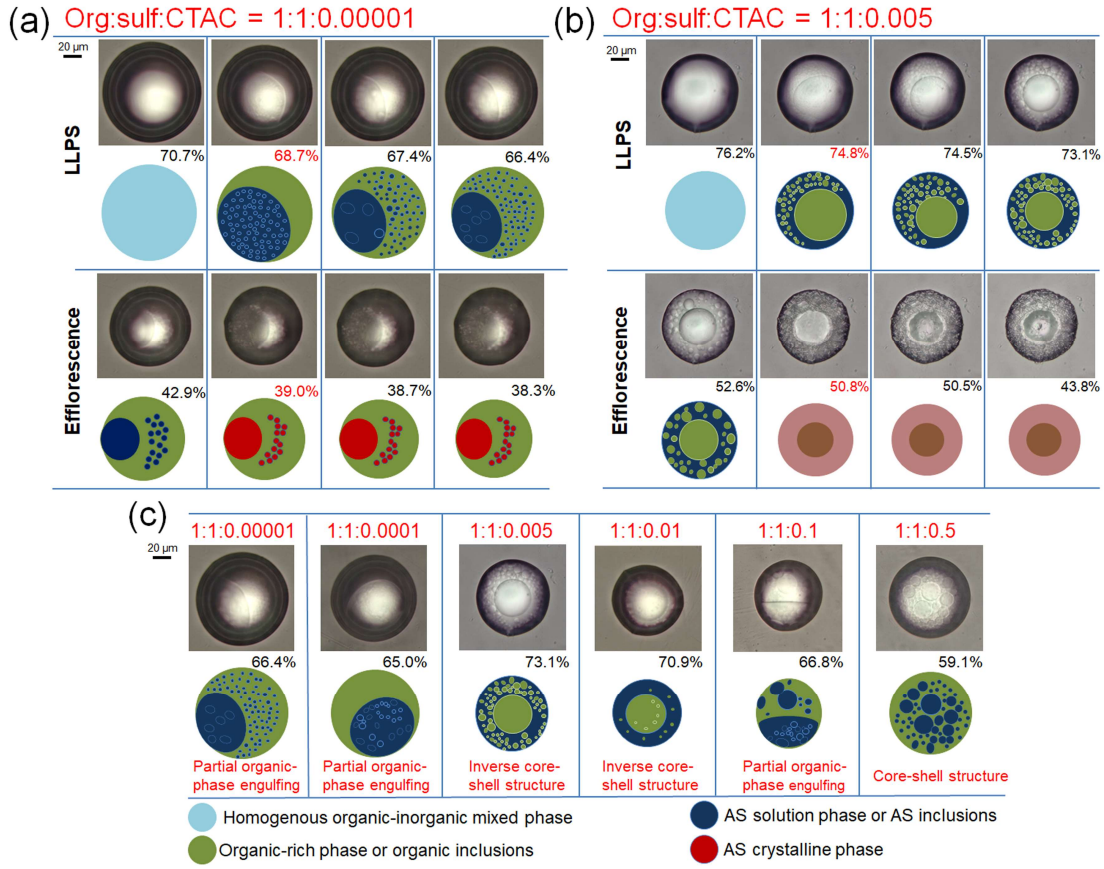

Figure S12. Optical images and corresponding illustrations of mixed 1,2,6-hexanetriol/AS/CTAC particles with org:sulf:CTAC ratios of 1:1:0.00001 (a) and 1:1:0.005 (b) during LLPS, efflorescence, and deliquescence. The RH percentage is indicated in each frame, with specific values highlighted in red to signify the occurrence of phase transitions. (c) Equilibrium particle morphologies after LLPS for 1,2,6-hexanetriol/AS/CTAC particles at different initial CTAC concentrations.

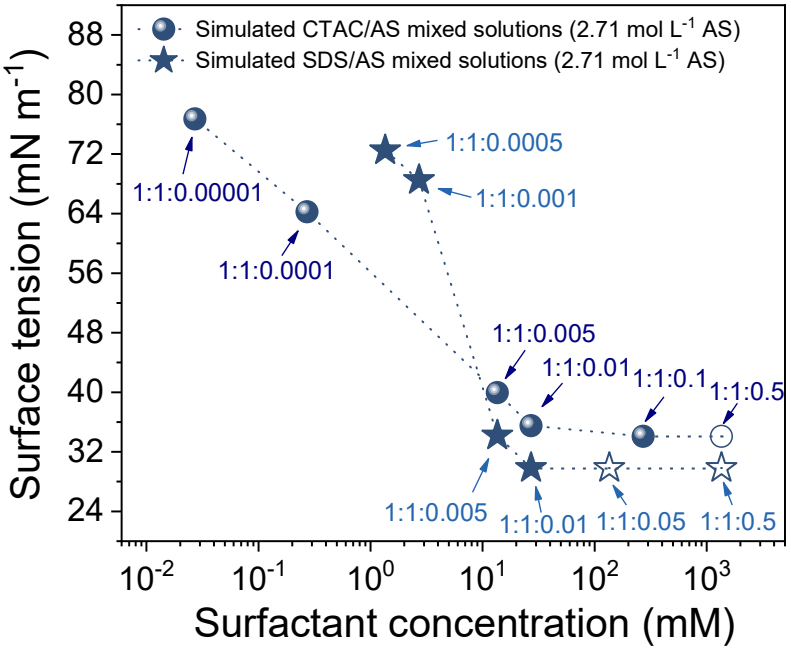

289

290 **Figure S13.** Surface tension measurements at varying concentrations of CTAC and SDS for

291 simulated CTAC/AS and SDS/AS mixed solutions, with a fixed AS concentration of 2.71 mol L^{-1}.

292 Hollow symbols indicate estimated approximate surface tension values.

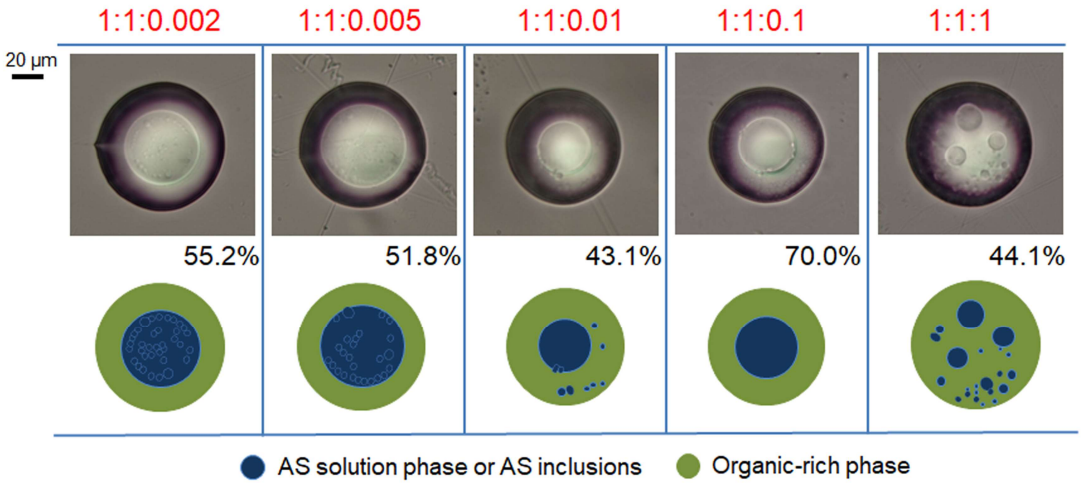

293

294 **Figure S14.** Optical images and corresponding illustrations of mixed 1,2,6-hexanetriol/AS/Triton

295 X-100 particles with varying org:sulf:Triton X-100 ratios after LLPS.

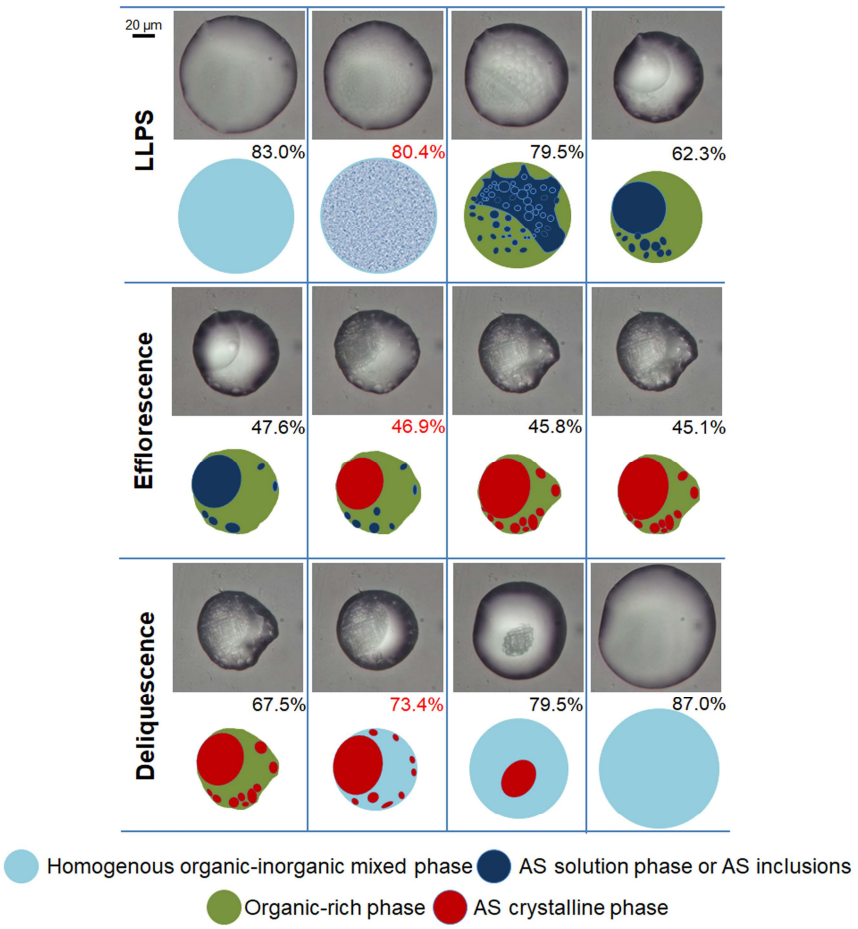

Figure S15. Optical images and corresponding illustrations of mixed 1,2,6-hexanetriol/AS/PFOA particles with the molar ratio of 1:1:0.1 during LLPS, efflorescence, and deliquescence. The RH percentage is indicated in each frame, with specific values highlighted in red to signify the occurrence of phase transitions.

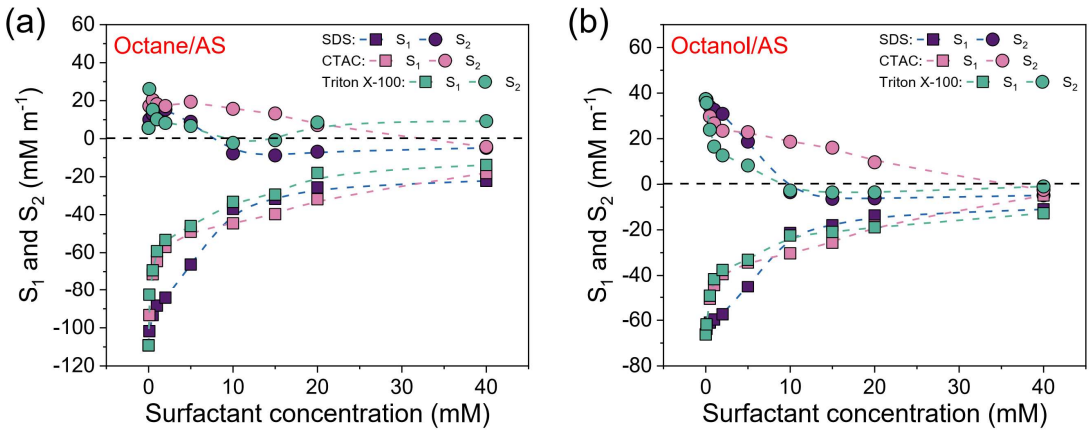

Figure S16. Calculated spreading coefficients, S_1 and S_2, as a function of surfactant concentration for model systems of octane/AS (a) and octanol/AS (b) with the addition of SDS, CTAC, or Triton X-100.

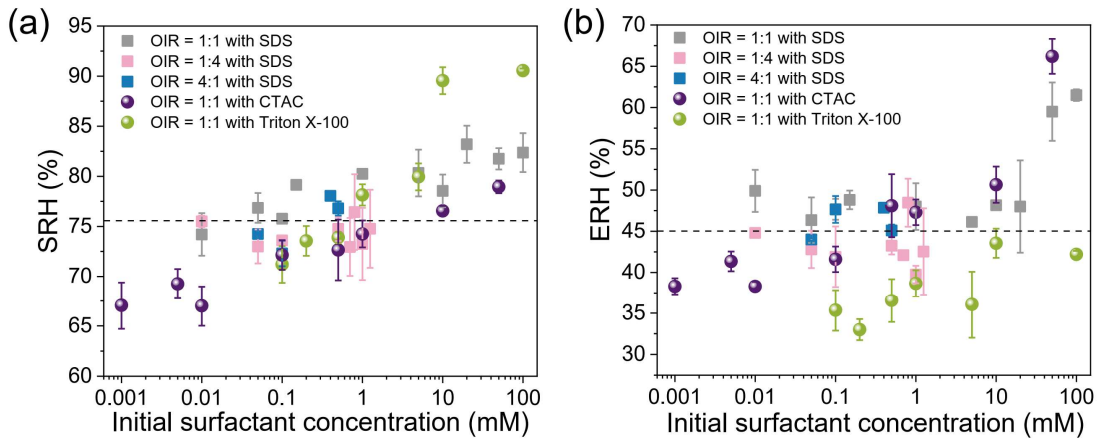

Figure S17. SRH (a) and ERH (b) values for OIR = 1:4, 1:1, and 4:1 particles with varying initial concentrations of SDS, CTAC, and Triton X-100. The dotted lines indicate the original SRH and ERH values for 1,2,6-hexanetriol/AS mixed particles without surfactants.

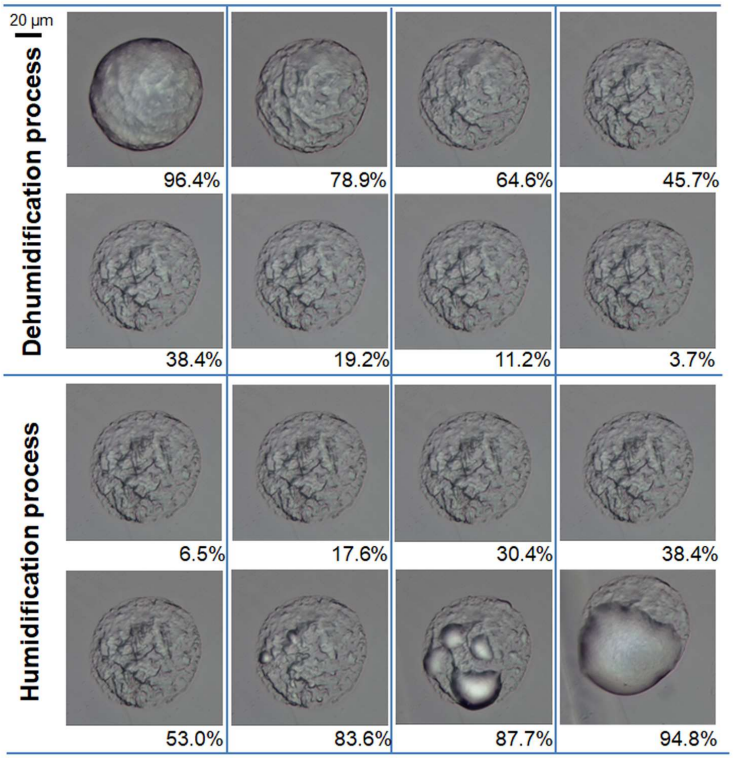

Figure S18. Optical images of pure SDS system during an RH cycle. The RH percentage is indicated in each frame.

References:

Boyer, H., Wexler, A., and Dutcher, C. S.: Parameter interpretation and reduction for a unified statistical mechanical surface tension model, J. Phys. Chem. Lett., 6, 3384-3389, https://doi.org/10.1021/acs.jpclett.5b01346, 2015.

Ciobanu, V. G., Marcolli, C., Krieger, U. K., Weers, U., and Peter, T.: Liquid-liquid phase separation in mixed organic/inorganic aerosol particles, J. Phys. Chem. A, 113, 10966-10978, https://doi.org/10.1021/jp905054d, 2009.

Dutcher, C. S., Wexler, A. S., and Clegg, S. L.: Surface tensions of inorganic multicomponent aqueous electrolyte solutions and melts, J. Phys. Chem. A, 114, 12216-12230, https://doi.org/10.1021/jp105191z, 2010.

Dutcher, C. S., Ge, X., Wexler, A. S., and Clegg, S. L.: Statistical mechanics of multilayer sorption: Extension of the Brunauer–Emmett–Teller (BET) and Guggenheim–Anderson–de Boer (GAB) adsorption isotherms, J. Phys. Chem. C, 115, 16474-16487, https://doi.org/10.1021/jp203879d, 2011.

Dutcher, C. S., Ge, X., Wexler, A. S., and Clegg, S. L.: An isotherm-based thermodynamic model of multicomponent aqueous solutions, applicable over the entire concentration range, J. Phys. Chem. A, 117, 3198-3213, https://doi.org/10.1021/jp310860p, 2013.

Faust, J. A., and Abbatt, J. P. D.: Organic surfactants protect dissolved aerosol components against heterogeneous oxidation, J. Phys. Chem. A, 123, 2114-2124, https://doi.org/10.1021/acs.jpca.9b00167, 2019.

Harmon, C. W., Grimm, R. L., Mcintire, T. M., Peterson, M. D., Njegic, B., Angel, V. M., Alshawa, A., Underwood, J. S., Tobias, D. J., and Gerber, R. B.: Hygroscopic growth and deliquescence of NaCl nanoparticles mixed with surfactant SDS, J. Phys. Chem. B, 114, 2435-2449, https://doi.org/10.1021/jp909661q, 2010.

Kwamena, N. O. A., Buajarern, J., and Reid, J. P.: Equilibrium morphology of mixed organic/inorganic/aqueous aerosol droplets: Investigating the effect of relative humidity and surfactants, J. Phys. Chem. A, 114, 5787-5795, https://doi.org/10.1021/jp1003648, 2010.

Ma, S., Chen, Z., Pang, S., and Zhang, Y.: Observations on hygroscopic growth and phase transitions of mixed 1, 2, 6-hexanetriol/$(NH_4)_2SO_4$ particles: investigation of the liquid–liquid phase separation (LLPS) dynamic process and mechanism and secondary LLPS during the dehumidification, Atmos. Chem. Phys., 21, 9705-9717, https://doi.org/10.5194/acp-21-9705-2021, 2021a.

Ma, S., Pang, S., Li, J., and Zhang, Y.: A review of efflorescence kinetics studies on atmospherically relevant particles, Chemosphere, 277, 130320, https://doi.org/10.1016/j.chemosphere.2021.130320, 2021b.

Miñambres, L., Méndez, E., Sánchez, M. N., Castaño, F., and Basterretxea, F. J.: The effect of low solubility organic acids on the hygroscopicity of sodium halide aerosols, Atmos. Chem. Phys., 14, 11409-11425, https://doi.org/10.5194/acp-14-11409-2014, 2014.

Prisle, N. L., Raatikainen, T., Laaksonen, A., and Bilde, M.: Surfactants in cloud droplet activation: mixed organic-inorganic particles, Atmos. Chem. Phys., 10, 5663-5683, https://doi.org/10.5194/acp-10-5663-2010, 2010.

Shaw, D. J.: Introduction to colloid and surface chemistry: 4th edition, Butterworth-Heinemann, Oxford, U.K., 1992.

Svenningsson, B., Rissler, J., Swietlicki, E., Mircea, M., Bilde, M., Facchini, M. C., Decesari, S., Fuzzi, S., Zhou, J., Mønster, J., and Rosenørn, T.: Hygroscopic growth and critical supersaturations for mixed aerosol particles of inorganic and organic compounds of atmospheric relevance, Atmos. Chem. Phys., 6,

1937-1952, https://doi.org/10.5194/acp-6-1937-2006, 2006.
Szyskowski, B. V.: Experimentelle studien über kapillare eigenschaften der wässerigen lösungen von fettsäuren, Zeitschrift für Physikalische Chemie, 64, 385-414, 1908.
Torza, S., and Mason, S. G.: Three-phase interactions in shear and electrical fields, J. Colloid Interface Sci., 33, 67-83, https://doi.org/10.1016/0021-9797(70)90073-1, 1970.
Wexler, A. S., and Dutcher, C. S.: Statistical mechanics of multilayer sorption: Surface tension, J. Phys. Chem. Lett., 4, 1723-1726, https://doi.org/10.1021/jz400725p, 2013.